Article
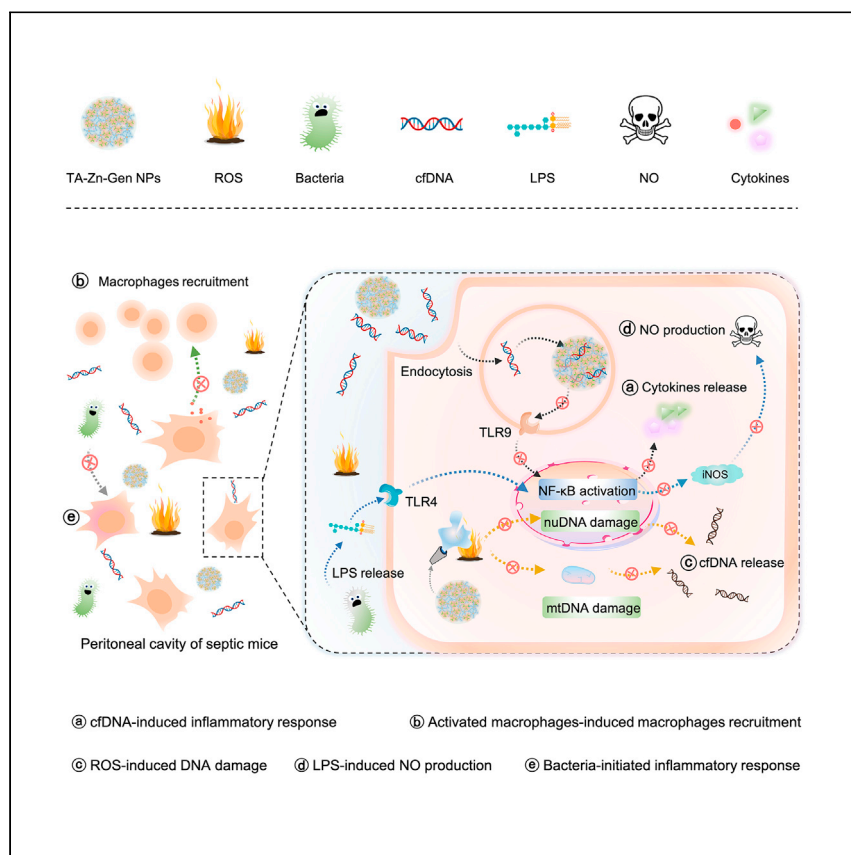
Targeting multiple mediators of sepsis using multifunctional tannic acid-Zn^{2+}-gentamicin nanoparticles

Feng Liu, Shu Sheng, Dan Shao, ..., Huayu Tian, Xuesi Chen, Kam W. Leong

thy@ciac.ac.cn (H.T.)
kam.leong@columbia.edu (K.W.L.)

Highlights

Design of multifunctional nanoparticles that can target multiple mediators of sepsis·

A new strategy of treating inflammatory disease with anionic therapeutic nanomaterials

Multifunctional TA-Zn-Gen NPs were developed for improved sepsis treatment. The TA-Zn-Gen NPs exerted their anti-sepsis activity by: (1) binding cfDNA with high affinity and inhibiting cfDNA-induced activation TLRs and nuclear factor kappa B signaling; (2) inhibiting macrophage recruitment; (3) scavenging reactive oxygen species (ROS) and reducing ROS-induced DNA damage and cell death; (4) inhibiting nitric oxide production induced by bacterial lipopolysaccharides; and (5) providing potent antibacterial activity, greater than that of an equivalent dose of free gentamicin.

Development

6

Practical, real world, technological considerations and constraints

Matter

CellPress

Article

Targeting multiple mediators of sepsis using multifunctional tannic acid-Zn^{2+}-gentamicin nanoparticles

Feng Liu,[1,2,3] Shu Sheng,[1,3] Dan Shao,[4] Yongqiang Xiao,[2] Yiling Zhong,[2] Jie Zhou,[2] Chai Hoon Quek,[2] Yanbing Wang,[1,5] Jianati Dawulieti,[4] Chao Yang,[4] Huayu Tian,[1,3,5,*] Xuesi Chen,[1,3,5] and Kam W. Leong[2,6,7,*]

SUMMARY

Treatments that target single mediators of sepsis have failed to reduce its high mortality rate. Here we developed multifunctional tannic acid-Zn^{2+}-gentamicin nanoparticles (TA-Zn-Gen NPs) that target multiple mediators of sepsis to improve sepsis treatment. TA-Zn-Gen NPs with lower gentamicin content possessed net negative surface charge but still bound cell-free DNA (cfDNA) with high affinity. The TA-Zn-Gen NPs exhibited five modes of anti-sepsis activity: (1) scavenged cfDNA and inhibited cfDNA-initiated activation of toll-like receptors and NF-κB signaling; (2) inhibited activated macrophage-induced macrophage recruitment; (3) scavenged reactive oxygen species (ROS) and reduced ROS-induced DNA damage and cell death; (4) inhibited nitric oxide production induced by lipopolysaccharides; and (5) potent antibacterial activity. The NPs reduced multiple organ damage and increased the survival rate of mice with severe sepsis. Together, the results demonstrate the potency of targeting multiple mediators for sepsis treatment, and support the development of multifunctional NPs for treating other intractable inflammation-related diseases.

INTRODUCTION

Sepsis is a life-threatening systemic inflammatory response to fungal, bacterial, or viral infection.[1,2] Despite advances in sepsis treatment, the mortality rate of sepsis remains high, and over eight million people die annually due to sepsis.[3] Recent efforts to develop more effective treatments of sepsis have focused on its pathogenesis,[4,5] and multiple mediators of sepsis that are essential to its onset and progression have been identified.[6–8] During the progression of sepsis, damage-associated molecular patterns (DAMPs) released by host cells and pathogen-associated molecular patterns (PAMPs) initiate inflammatory reactions that can cause a "cytokine storm," multiple organ failure, and death.[9,10] Inflammatory circulating cell-free DNA (cfDNA)—nuclear or mitochondrial DNA released by damaged host cells—is one such DAMP, and activates immune cells via toll-like receptor (TLR) activation, eliciting a sterile inflammatory response.[11–13] Cationic nanoparticles (NPs) have been explored for scavenging inflammatory anionic cfDNA to treat cfDNA-associated diseases,[14–17] but their potential systemic cytotoxicity would limit their clinical use.[18] Other mediators of sepsis include lipopolysaccharides (LPSs) released from the membranes of infectious bacteria. LPSs are potent PAMPs that activate immune cell TLRs, stimulating the production of nitric oxide (NO) and inflammatory cytokines.[19–21] Antagonists of TLR activation can reduce inflammation in sepsis, but

Progress and potential

Recent research points to the pathogenic role of cell-free DNA (cfDNA) as damage-associated molecular pattern molecules in activating the toll-like receptor (TLR) pathways and inducing inflammation. We, and others, have been using cationic nanostructures to scavenge cfDNA molecules as a new strategy to modulate sepsis. To reduce toxicity, we hypothesize that the incorporation of antibacterial and antioxidation components into an anion nanostructure can offer the multifunctionality of cfDNA scavenging, antibacterial effect, and antioxidation to improve therapeutic efficacy while reducing side effects. We screened a number of nanoparticle (NP) compositions and showed that the tannic acid-Zn^{2+}-gentamicin NPs (TA-Zn-Gen NPs) with multiple anti-sepsis activity could reduce multiple organ damage and achieve a 60% survival rate in a severe sepsis animal model. Our study suggests a new strategy of treating inflammatory diseases with anionic nanomaterials.

CellPress

Matter
Article

excessive TLR inhibition and systemic loss of TLR function can cause immune suppression and increase the risk of infection.[22–24] Excessive production of reactive oxygen species (ROS) such as hydroxyl radicals (•OH) and superoxide anion radicals ($O_2^{•-}$) also plays an important role in sepsis.[25,26] Increased ROS levels cause DNA damage resulting in loss of cell function, cell death, and release of cfDNA,[27] perpetuating systemic inflammation and leading to organ failure and death. Reducing ROS levels is thus critical in sepsis treatment.

Therapies that target only a single mediator of sepsis have failed to reduce its mortality rate.[28–31] Since multiple factors contribute dynamically to cause systemic inflammation during sepsis,[32] we hypothesized that a multifunctional NP that targeted multiple factors simultaneously could achieve a greater anti-sepsis therapeutic effect. Here, we developed multifunctional TA-Zn-Gen NPs that consist of tannic acid, Zn^{2+}, and gentamicin for improved sepsis treatment. We synthesized a series of TA-Zn-Gen NPs with different gentamicin contents in a simple, low-cost, scalable, one-pot process at ambient temperature (Figure 1A), and characterized the NPs in terms of their physicochemical properties and anti-sepsis therapeutic activity *in vitro* and *in vivo*, with a focus on five mechanisms of anti-sepsis therapeutic activity (Figures 1B and 1C): (1) binding and scavenging inflammatory cfDNA and inhibition of cfDNA-induced TLR activation and NF-κB signaling; (2) inhibition of activated macrophage-induced macrophage recruitment; (3) scavenging of ROS and inhibition of ROS-induced DNA damage and cell death; (4) inhibition of bacterial LPS-induced NO production; and (5) antibacterial activity and inhibition of bacteria-induced inflammation.

RESULTS AND DISCUSSION
Characterization of TA-Zn-Gen NPs
We fabricated a series of TA-Zn-Gen NPs with increasing amounts of gentamicin (Table S1). The chemical structures of tannic acid and gentamicin are shown in Figure S1. As-constructed TA-Zn-Gen NPs displayed spherical morphology (Figure S2). The size, polydispersity index (PDI), and zeta potential of the NPs increased with increasing gentamicin content (Figures 2A–2C). Intriguingly, when the tannic acid/gentamicin (TA:Gen) weight ratio was increased from 1:0.5 to 1:1, the NP size increased sharply from ∼200 nm to over 2 μm in diameter, and the surface charge flipped from negative to positive. Since anionic NPs are favorable for prolonging blood circulation time and enhancing accumulation in inflamed sites,[33] we selected the three smaller, anionic NPs for further investigation. Element analysis confirmed the presence of nitrogen (due to gentamicin) in the NPs (Figure 2D), and inductively coupled plasma mass spectroscopy (ICP-MS) confirmed the presence of Zn (Figure 2D). C=O and C=C characteristic peaks of tannic acid[34] were observed in the Fourier transform infrared spectroscopy (FTIR) spectra of the NPs (Figure 2E), confirming the presence of tannic acid. No crystalline peak was observed in X-ray diffraction (XRD) spectra (Figure 2F), indicating an amorphous structure. Stability analysis of the TA-Zn-Gen NPs showed no statistically significant change in size after 2 days of incubation in phosphate buffered solution (PBS), Fetal bovine serum (FBS), or Dulbecco's modified Eagle's medium (DMEM) containing 10% FBS, indicating their stability under physiological condition (Figure S3).

DNA binding affinity of TA-Zn-Gen NPs
In preliminary experiments, we were surprised to observe that TA-Zn-Gen NPs with a net negative surface charge (NPs 1–3) exhibited concentration-dependent absorption of Cy5-labeled CpG (a short single-stranded DNA [ssDNA] oligonucleotide that activates TLR9) (Figure S4). We further evaluated the calf thymus DNA binding affinity of the NPs in Tris-EDTA (TE) buffer with and without 10% FBS by measuring

[1]Key Laboratory of Polymer Ecomaterials, Changchun Institute of Applied Chemistry, Chinese Academy of Sciences, Changchun 130022, China

[2]Department of Biomedical Engineering, Columbia University, New York 10027, USA

[3]University of Chinese Academy of Sciences, Beijing 100049, China

[4]Institutes for Life Sciences, School of Biomedical Sciences and Engineering, South China University of Technology, Guangzhou International Campus, Guangzhou, 510006, China

[5]University of Science and Technology of China, Hefei 230026, China

[6]Department of Systems Biology, Columbia University, New York 10032, USA

[7]Lead contact

*Correspondence: thy@ciac.ac.cn (H.T.), kam.leong@columbia.edu (K.W.L.)

https://doi.org/10.1016/j.matt.2021.09.001

Matter
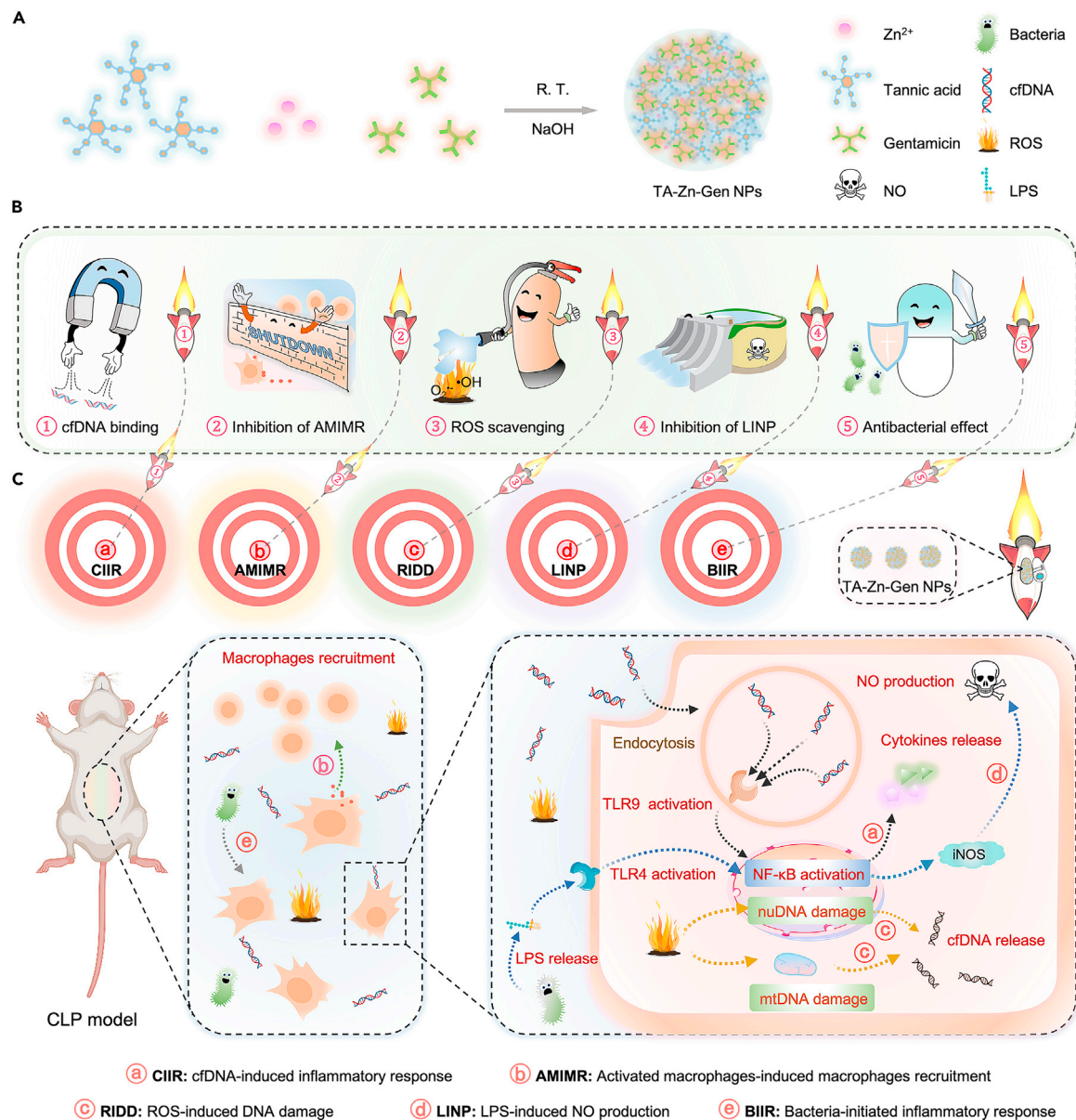**Article**

CellPress

Figure 1. Schematic illustration of preparation of TA-Zn-Gen NPs and using TA-Zn-Gen NPs to treat sepsis
(A) Preparation of TA-Zn-Gen NPs.
(B) Schematic of anti-sepsis therapeutic targets of the NPs.
(C) Mechanistic view of anti-sepsis activity of NPs in a CLP-induced sepsis model. The therapeutic targets (a–e) are defined at the bottom of the figure.

unbound PicoGreen-labeled DNA (Figures 3A and 3B). Despite their net negative surface charge, TA-Zn-Gen NPs 1–3 exhibited high DNA binding affinity. TA-Zn-Gen NPs with increasing gentamicin content displayed increasing DNA binding affinity, possibly due to electrostatic interactions between DNA and gentamicin. Interestingly, free tannic acid also exhibited DNA binding (Figure 3A), possibly due to hydrogen bonding between tannic acid and the phosphate backbone of DNA. The addition of 10% FBS reduced DNA binding in all groups, but the competitive interactions due to serum proteins were overcome by increasing the amount of NPs (Figure 3B). To investigate whether charged molecules in the cytoplasm of cells cause dissociation of TA-Zn-Gen/DNA complexes, we performed GFP plasmid
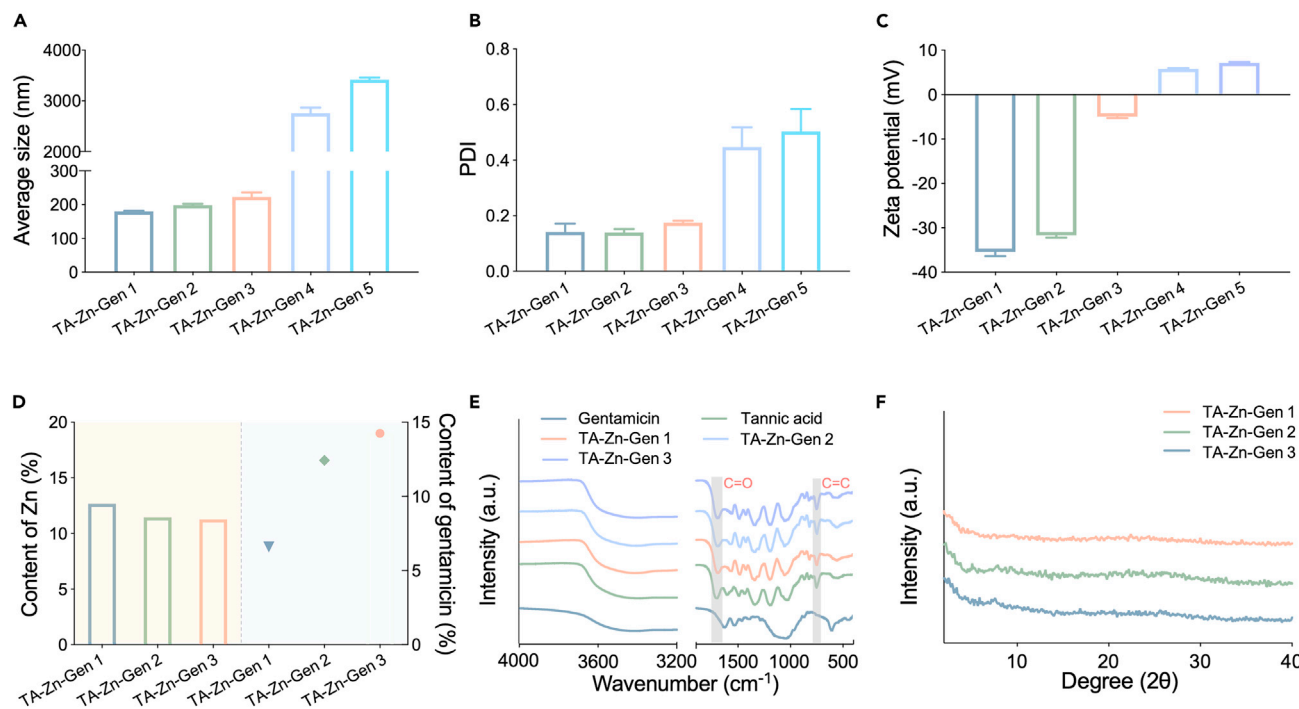
CellPress

Matter
Article

Figure 2. Characterization of TA-Zn-Gen NPs

(A–C) (A) Size, (B) PDI, and (C) zeta potential of TA-Zn-Gen NPs with increasing gentamicin content. TA:Gen weight ratio = (1) 1:0.125, (2) 1:0.25, (3) 1:0.5, (4) 1:1, (5) 1:2. A sharp increase in particle size and PDI and a change from net negative to positive surface charge occurred between a TA:Gen weight ratio of 1:0.5 and 1:1.

(D–F) (D) ICP-MS and element analysis, (E) FTIR spectra, and (F) XRD spectra of TA-Zn-Gen NPs 1–3.

transfection experiments using TA-Zn-Gen 3 NPs as a plasmid DNA carrier. A CCK-8 assay was used to determine the cytotoxicity of the NPs to RAW 264.7 murine macrophage cells (Figure 3C), and a nontoxic NPs concentration of 100 μg/mL was chosen for transfection experiments. Following transfection of HEK 293 cells, bright fluorescence was observed in the positive control group (using Lipofectamine 3000 as DNA carrier), but negligible fluorescence was observed when TA-Zn-Gen 3 NPs were used as the DNA carrier (Figure S5). These results suggest that robust binding between the NPs and plasmid prevented release of the GFP-encoding plasmid for transcription and translation.

Anti-inflammatory effect of TA-Zn-Gen NPs *in vitro*

Inflammatory circulating nucleic acids such as CpG DNA activate TLR9 signaling following endocytosis, leading to recruitment of MyD88 and NF-κB signaling.[35] Therefore, we investigated the internalization of the TA-Zn-Gen NPs and their ability to block CpG-induced TLR9 activation *in vitro*. FITC-labeled TA-Zn-Gen NPs were internalized with high efficiency by RAW 264.7 cells, as observed by confocal laser scanning microscopy (CLSM) (Figures 3D and S6). Colocalization of FITC-labeled NPs and Cy5-CpG fluorescence was observed in endolysosomal compartments (Figure 3D), confirming the internalization of TA-Zn-Gen NPs via endocytosis, which might be beneficial for blocking recognition between CpG and TLR9.

We then measured NP inhibition of nucleic acid-induced TLR activation by using HEK-Blue human TLR (hTLR) cells and monitoring downstream NF-κB signaling (Figure S7). HEK-Blue hTLR3, hTLR4, and hTLR9 cells were constructed by co-transfecting the hTLR gene and an optimized secreted embryonic alkaline
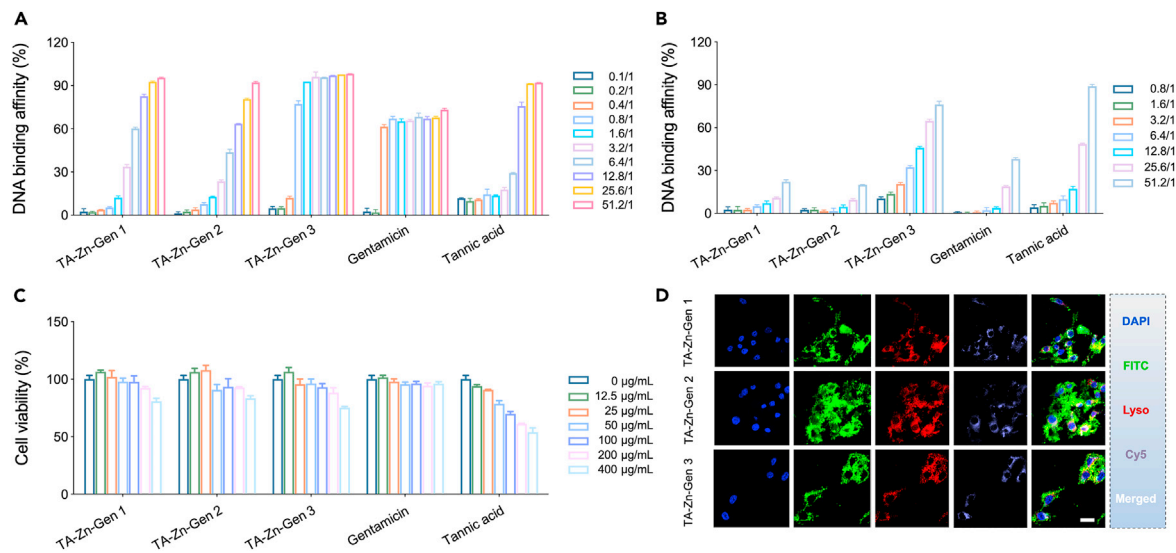
Figure 3. DNA binding affinity and cytotoxicity

(A and B) DNA binding affinity of NPs at different NP:DNA mass ratios (see legend) in TE buffer without FBS (A) and with 10% FBS (B). [Calf thymus DNA] = 0.5 µg/mL.

(C) Cytotoxicity of NPs to RAW 264.7 cells.

(D) Colocalization of FITC-labeled TA-Zn-Gen NPs and Cy5-labeled CpG in lysosomes (CLSM images). Scale bar, 10 µm.

phosphatase (SEAP) reporter gene into HEK 293 cells. An IFN-β minimal promoter fused to five NF-κB and AP-1 binding sites was designed to control the expression of SEAP reporter gene. TLR agonist treatments initiate the expression of NF-κB and AP-1, which induce production of SEAP, which is detected by using Quanti-Blue reagent and measuring the optical density (OD) at 620 nm. We tested three TLR agonists: (1) CpG Bw006 ssDNA oligonucleotide, a TLR9 ligand; (2) Poly (I:C), a synthetic double-stranded RNA analog that activates TLR3 signaling; and (3) LPS, a TLR4 ligand. The NPs alone did not activate the TLRs (Figure S8). Consistent with the previous nucleic acid binding results, the NPs inhibited CpG-induced activation of HEK-Blue hTLR9 cells and inhibited Poly (I:C)-induced activation of HEK-Blue hTLR3 cells in a NP dose-dependent manner, regardless of the presence or absence of FBS (Figures 4A, 4B, 4D, 4E, and S9). However, the NPs did not inhibit LPS-induced HEK-Blue hTLR4 activation (Figures 4C and 4F). Together, these results demonstrate that the TA-Zn-Gen NPs specifically inhibit nucleic acid (DNA or RNA but not LPS)-induced TLR activation and downstream NF-κB signaling.

To our surprise, tannic acid alone also inhibited nucleic acid-induced activation of TLR9 and TLR3. We then performed a further experiment to prove that the anti-inflammation activity of TA-Zn-Gen NPs was derived from the nucleic acid scavenging capability instead of the function of tannic acid. In this experiment, we mixed each agonist (CpG, Poly (I:C), or LPS) with TA-Zn-Gen NPs at different NPs concentrations for 1 h, then centrifuged the mixture to precipitate TA-Zn-Gen/agonist complexes, and used the supernatant to treat HEK-Blue hTLR cells. When a high NP concentration was used, the supernatant treatment resulted in lower levels of HEK-Blue hTLR9 and hTLR3 cell activation (Figure S10). This result indicated that NP inhibition of TLR activation was derived from nucleic acid scavenging (Figure 4G).

Activation of TLR9 by inflammatory circulating cfDNA has been suggested to play a critical role in the progression of sepsis.[36–38] We next used CpG Bw006 to initiate TLR9 activation in RAW 264.7 cells and evaluated the anti-inflammation effect of the
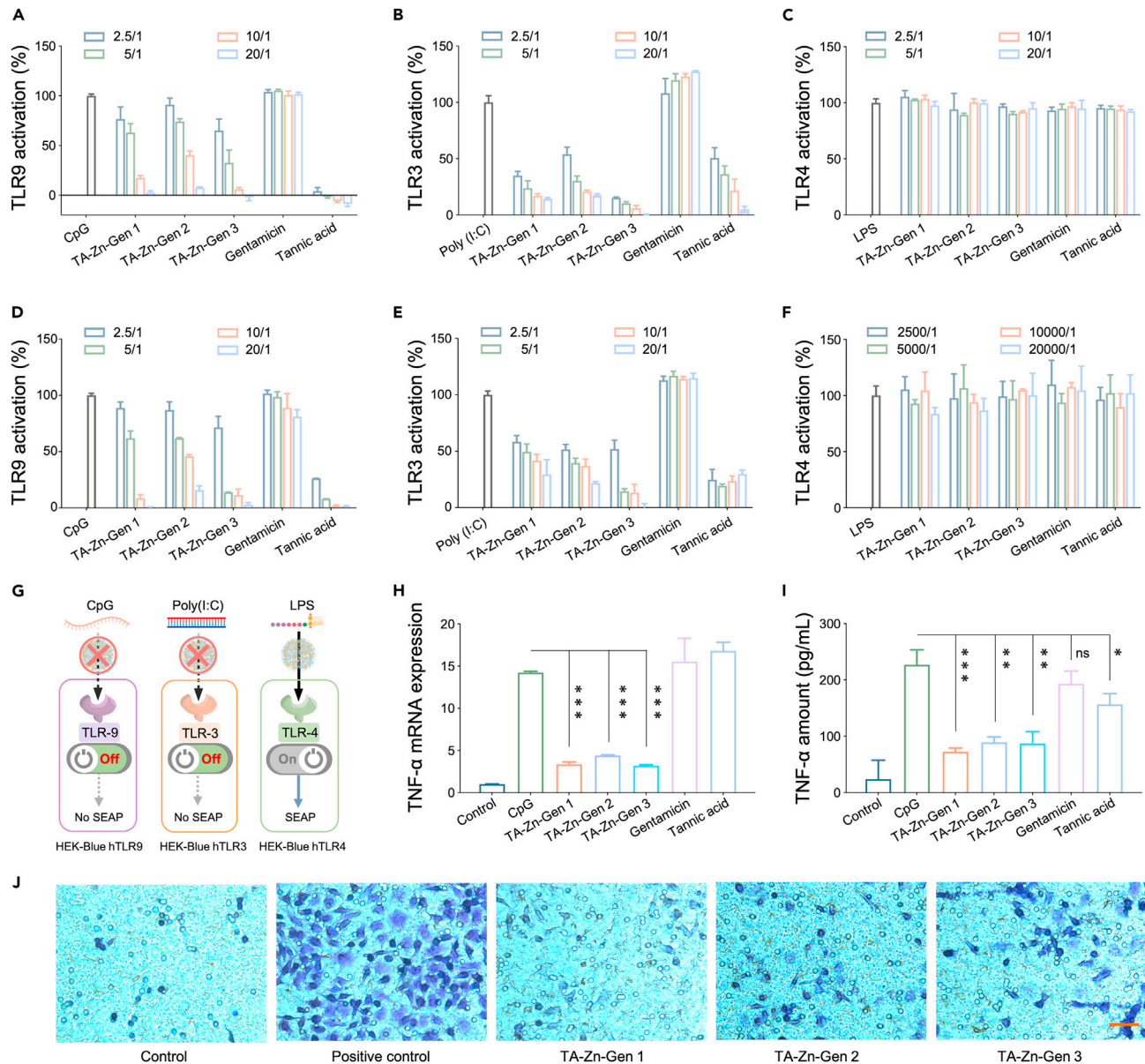
Figure 4. Inhibition of nucleic acid-induced TLR activation and activated macrophage-induced macrophage migration

(A–F) Activation of HEK-Blue (A) hTLR9, (B) hTLR3, and (C) hTLR4 cells in the absence of FBS after different treatments for 24 h. Activation of HEK-Blue (D) hTLR9, (E) hTLR3, and (F) hTLR4 cells in the presence of FBS after different treatments for 24 h. The legend indicates NPs:agonist mass ratios.

(G) Schematic of inhibition of nucleic acid-induced TLR activation by TA-Zn-Gen NPs.

(H and I) (H) TNF-α mRNA and (I) TNF-α cytokine generated by macrophages after different treatments for 24 h.

(J) Inhibition of activated macrophage-induced macrophage migration, measured using a transwell assay. Data are expressed as mean ± SD. Statistical comparisons of groups were performed using a Student's t test (*p < 0.05, **p < 0.01, ***p < 0.001).

TA-Zn-Gen NPs in terms of tumor necrosis factor alpha (TNF-α) transcription and translation. TA-Zn-Gen NP treatment reduced transcription and translation of TNF-α (Figures 4H and 4I), indicating NPs inhibition of nucleic acid-induced inflammation *in vitro*.

Inhibition of activated macrophages-induced macrophages recruitment

Macrophage accumulation in inflamed sites aggravates inflammation, and reducing activated macrophage-induced macrophage recruitment is a promising strategy for

alleviating inflammation in sepsis.[39] CpG Bw006-activated RAW 264.7 macrophages recruited a large number of macrophages from the upper side of a transwell chamber to the lower side (Figures 4J and S11) due to chemotaxis induced by release of attractants by activated macrophages. When TA-Zn-Gen NPs were added, macrophage migration was sharply reduced. Thus, the TA-Zn-Gen NPs not only inhibit nucleic acid-initiated TLR activation but also inhibit activated macrophage-induced macrophage migration once macrophages are activated.

ROS scavenging and protection from ROS-induced cell damage

ROS have emerged as an important factor in the pathophysiology of sepsis.[40] Since tannic acid is a natural antioxidant that has been explored for use as an ROS scavenger, we examined the ROS scavenging ability of TA-Zn-Gen NPs. The •OH scavenging capability of the TA-Zn-Gen NPs was assessed by monitoring the absorption kinetics at 650 nm of oxidized 3,3′,5,5′-tetramethylbenzidine (TMB) generated from the oxidation of TMB by •OH. A Fenton reaction between Cu^{2+} and H_2O_2 was used to produce •OH. The TA-Zn-Gen NPs markedly reduced the generation of oxidized TMB by •OH in a NPs dose-dependent manner (Figures 5A and S12), indicating that the NPs scavenge hydroxyl radicals. Next, the oxidation of xanthine by xanthine oxidase was used to produce $O_2^{\bullet-}$, and the $O_2^{\bullet-}$ scavenging ability of the TA-Zn-Gen NPs was characterized by measuring the fluorescence of ethidium, the product of hydroethidine oxidation by $O_2^{\bullet-}$ at 610 nm.[41] The fluorescence intensity decreased with increasing NP concentration (Figure 5B), indicating the elimination of $O_2^{\bullet-}$ by the NPs. The intracellular ROS level was then evaluated by using cell-permeant 2′,7′-dichlorodihydrofluorescein diacetate (H_2DCFDA) as an indicator. Bright green fluorescence was observed in *tert*-butyl hydroperoxide (TBHP)-treated cells upon stimulation (Figures 5C and 5D), demonstrating the successful induction of oxidation pressure. With the introduction of the TA-Zn-Gen NPs, the fluorescence intensity in cells decreased significantly, indicating ROS scavenging by the NPs *in vitro*, which was further confirmed by detecting the 2′,7′-dichlorofluorescein (DCF) fluorescence at 520 nm with multiwell plate reader via excitation at 490 nm (Figure S13).

Next, the effect of TA-Zn-Gen NPs on ROS-induced cell DNA damage was evaluated through a plasmid nicking assay.[42] In this experiment, 2,2′-azobis(2-amidinopropane) dihydrochloride (AAPH) was used as an ROS source to convert supercoiled DNA into the nicked form. Supercoiled DNA and nicked DNA possess different electrophoretic mobilities and can be separated by agarose gel electrophoresis. The supercoiled plasmid DNA strand was damaged by AAPH treatment, and a high fraction of the nicked form was observed in a gel electrophoretogram (Figures 5E and S14). In contrast, the formation of the nicked form decreased dramatically when TA-Zn-Gen NPs were added, demonstrating protection from ROS-induced DNA damage by the NPs. Next, NP protection against cellular DNA damage was determined by measuring the amount of phosphorylation of the histone variant H_2AX.[43] TA-Zn-Gen NP-treated cells exhibited lower amounts of phosphorylated H_2AX (γH_2AX) than untreated cells (Figures 5F, S15, and S16), demonstrating the protective effect of the NPs on DNA integrity. Next, the protective effect of the TA-Zn-Gen NPs from ROS-induced cell death was investigated. The NPs reduced ROS-induced cell death in a dose-dependent manner (Figure 5G). Collectively, these results show that the TA-Zn-Gen NPs scavenge intracellular ROS and prevent ROS-induced DNA damage and cell death. This blocking of ROS-related inflammatory macrophage signaling is an important anti-sepsis activity.
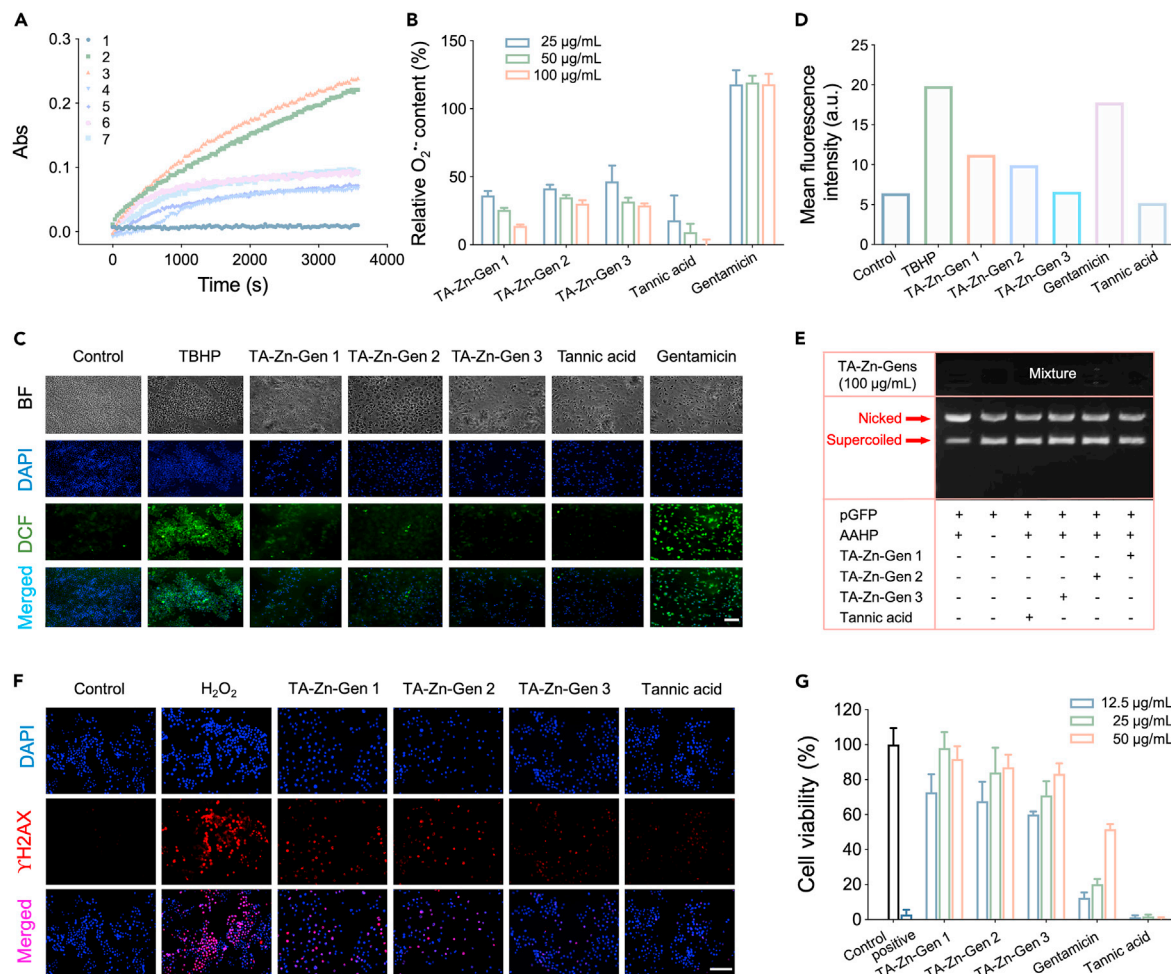
Figure 5. ROS scavenging capability and protection on ROS-induced DNA damage and cell death

(A and B) (A) •OH and (B) $O_2^{\cdot-}$ scavenging capability of the TA-Zn-Gen NPs. (A) 1, HT; 2, HTC; 3, HTC/gentamicin; 4, HTC/tannic acid; 5, HTC/TA-Zn-Gen 1; 6, HTC/TA-Zn-Gen 2; 7, HTC/TA-Zn-Gen 3. T, TMB; H, H_2O_2; C, Cu^{2+}.

(C) Intracellular ROS imaging of macrophages after treatments. BF, bright field. Scale bar, 100 μm.

(D) Semi-quantitative fluorescence intensity of images in Figure 5C evaluated by Image J.

(E) NPs protection from ROS-induced DNA damage assessed using a plasmid nicking assay and agarose gel electrophoresis. The positions of lanes from gels were rearranged to make them easy to compare.

(F) Phosphorylated histone variant H_2AX imaging of macrophages following different treatments. Scale bar, 100 μm.

(G) Protective effect of NPs on ROS-induced cell death (CCK-8 assay). Data are expressed as mean ± SD. Statistical comparisons of groups were performed using Student's t test (*p < 0.05, **p < 0.01, ***p < 0.001).

Inhibition of LPS-induced nitric oxide generation

LPS are potent PAMPs that are released from the outer membrane of bacteria and activate TLR4 on immune cells, eliciting the production of NO. Macrophage-derived NO plays a critical role in immune system protection against pathogenic infection. However, overexpression of NO by inducible nitric oxide synthase (iNOS) contributes to an excessive inflammation in sepsis.[44] Therefore, reduction of NO is an alternative strategy for mitigating inflammation in sepsis. Although the TA-Zn-Gen NPs did not specifically bind LPS and inhibit LPS-induced TLR4 activation, they did reduce LPS-stimulated iNOS mRNA expression and NO production in RAW 264.7 cells (Figures 6A and 6B).
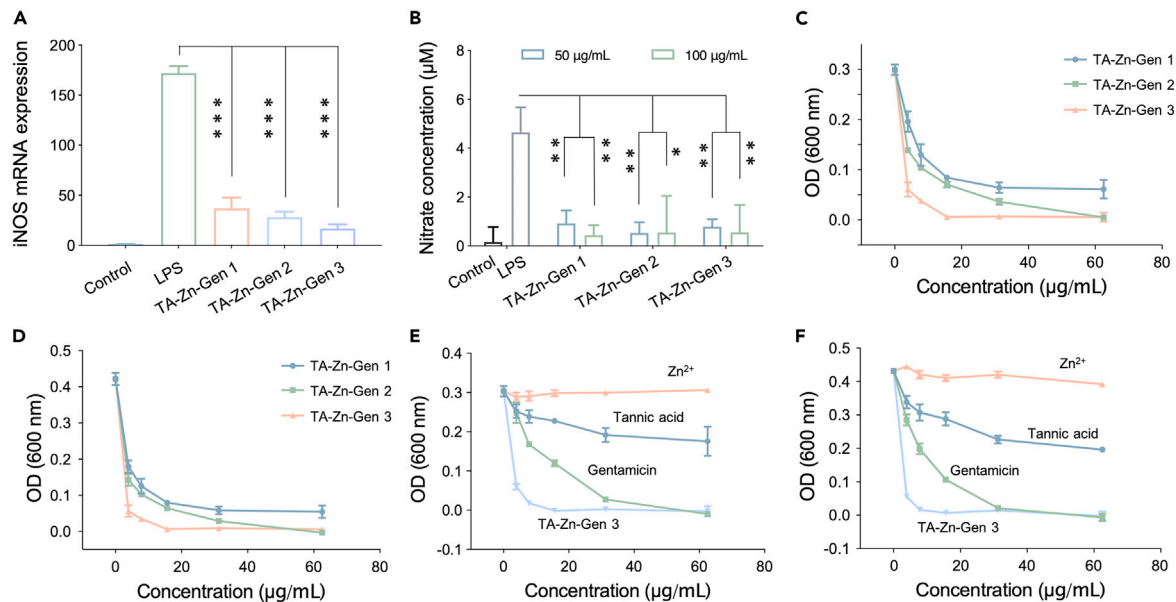
Figure 6. Inhibition of LPS-induced NO production and antibacterial effect
(A) Expression of iNOS mRNA in macrophages following different treatments.
(B) Level of NO generated by macrophages following different treatments.
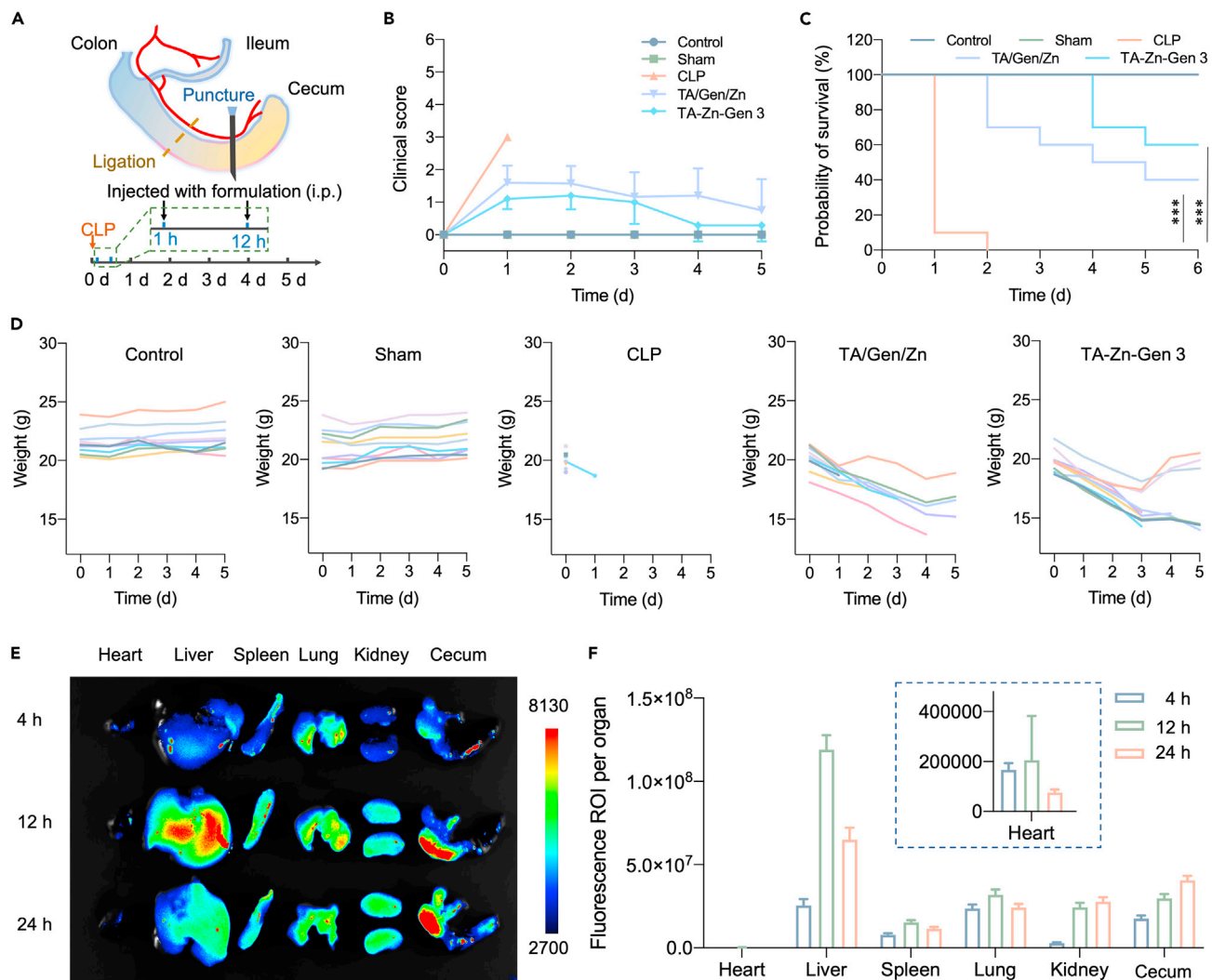(C and D) Antibacterial effect of TA-Zn-Gen NPs 1–3 after treatment for 6 h (C) and 12 h (D).
(E and F) Antibacterial effect of free tannic acid, free gentamicin, and TA-Zn-Gen 3 NPs after treatment for 6 h (E) and 12 h (F). Data are expressed as mean ± SD. Statistical comparisons of groups were performed using Student's t test (*p < 0.05, **p < 0.01, ***p < 0.001).

Antibacterial effect

To examine the direct effect of the TA-Zn-Gen NPs on pathogenic bacteria, we tested the effect of the NPs on *Escherichia coli*. TA-Zn-Gen NPs 1–3 (which have increasing gentamicin content) displayed increasing antibacterial activity at the same NPs concentration, indicating a gentamicin concentration-dependent antibacterial effect (Figures 6C, 6D, and S17). Since TA-Zn-Gen 3 NPs exhibited the strongest antibacterial activity, we selected these NPs for comparisons with the free components of the NPs. Free tannic acid exhibited slight antibacterial activity at a high concentration, and free gentamicin showed a potent concentration-dependent antibacterial effect (Figures 6E and 6F). Interestingly, TA-Zn-Gen 3 NPs exhibited greater antibacterial activity than free gentamicin and free tannic acid at the same dose, possibly due to a synergistic effect of gentamicin and tannic acid.

Anti-sepsis therapeutic activity of TA-Zn-Gen NPs in CLP-induced sepsis model

We selected the TA-Zn-Gen 3 NPs for *in vivo* studies because they showed the greatest DNA scavenging effect and antibacterial capability *in vitro*. We compared the anti-sepsis activity of the TA-Zn-Gen 3 NPs with that of a soluble mixture of the components of the NPs (TA/Gen/Zn) with an equivalent dosage of each component as in the NPs. A cecal ligation and puncture (CLP) procedure was implemented to establish polymicrobial peritonitis-induced sepsis (Figure 7A) due to this model's massive TLR9 activation, similar to clinical sepsis. CLP-induced severe sepsis was established in C57 mice as described previously.[45] The clinical score, survival rate, and body weight of mice were recorded for five consecutive days post CLP. Clinical score criteria are listed in the supporting information, in the section "treatment of CLP-induced sepsis model." The TA/Gen/Zn and TA-Zn-Gen 3 NP treatment groups exhibited significantly diminished clinical score (Figure 7B), indicating recovery of physical state after treatment. No mice in the CLP group without treatment survived

CellPress

Matter
Article

Figure 7. Therapeutic effect on CLP-induced sepsis
(A) Schematic of CLP-induced sepsis model and treatment schedule.
(B–D) (B) Clinical score, (C) survival rate, and (D) body weight of mice in different treatment groups recorded for five consecutive days.
(E and F) (E) *Ex vivo* fluorescence imaging and (F) quantitative assessment of distribution of Cy7-labeled TA-Zn-Gen 3 NPs in major organs and cecum at different times following CLP.
Data are expressed as mean ± SD. Statistical comparisons of groups were performed using a Student's t test (*p < 0.05, **p < 0.01, ***p < 0.001).

after 2 days. Repetitive intraperitoneal administration with TA/Gen/Zn at 1 h and 12 h post CLP resulted in a notable survival rate (40%) (Figure 7C). The same administration of TA-Zn-Gen 3 NPs further delayed CLP-induced lethality and produced the highest survival rate (60%). This result may be due to the scavenging of multiple mediators of sepsis by the NPs and their prolonged circulation and tissue retention time, improving their protection from organ damage. Increased mouse body weight was observed after 2 days of treatment with TA/Gen/Zn or TA-Zn-Gen 3 NPs (Figure 7D), further indicating an anti-sepsis therapeutic effect. The biodistribution and retention time of the TA-Zn-Gen 3 NPs was assessed by using fluorescent Cy7-labeled TA-Zn-Gen 3 NPs and *ex vivo* fluorescence imaging. The NPs were injected at 1 h after CLP, and the major organs and cecum were harvested at 4 h, 12 h, and 24 h post CLP for fluorescence imaging. TA-Zn-Gen 3 NPs showed long retention in major organs and inflamed cecum (Figures 7E and 7F), a promising result for
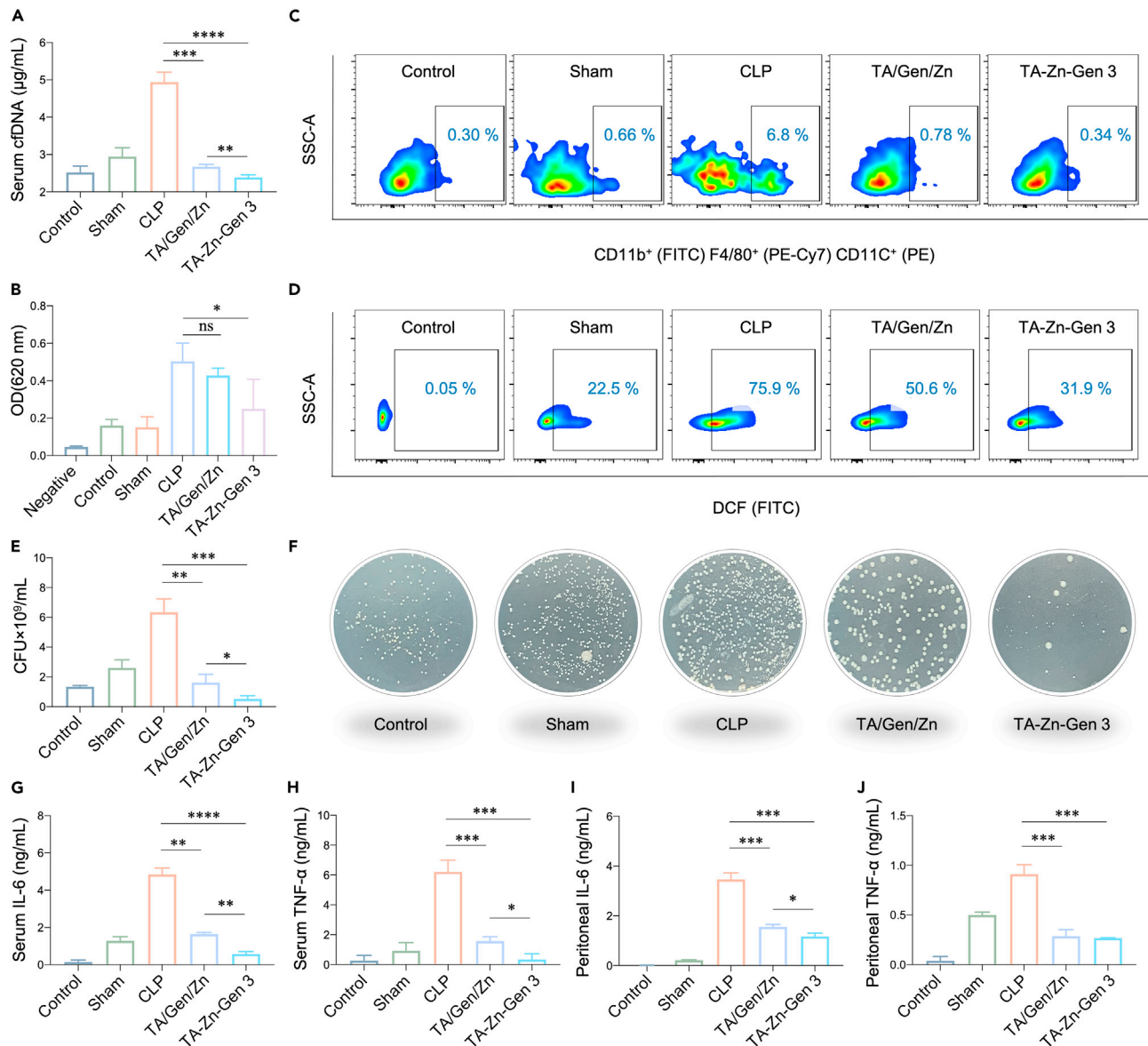
Figure 8. Effect on multiple meditators of sepsis *in vivo*

(A) Level of cfDNA in serum at 24 h post CLP.

(B) Activation of HEK-Blue hTLR9 cells in different treatment groups.

(C) M1 polarization ratio of macrophages.

(D) Cells with high ROS level in peritoneal cavity at 24 h post CLP, characterized by flow cytometry.

(E and F) (E) Bacteria CFU and (F) bacterial colony image from peritoneal cavity of mice in different treatment groups.

(G and H) Proinflammatory cytokines TNF-α (G) and IL-6 (H) in serum.

(I and J) TNF-α (I) and IL-6 (J) in peritoneal cavity. Data are expressed as mean ± SD. Statistical comparisons of groups were performed using Student's t test (*p < 0.05, **p < 0.01, ***p < 0.001).

prolonged protection from inflammatory mediators of sepsis and multiorgan dysfunction.

We further examined the effects of the NPs on multiple meditators of sepsis *in vivo*: cfDNA, activated macrophages, ROS, bacteria, and inflammatory cytokines. The untreated CLP group exhibited a sharply elevated cfDNA level in plasma and significantly increased activation of HEK-Blue hTLR9 cells by cfDNA extracted from serum

CellPress

Matter
Article

(Figure S18), in contrast to control and sham groups. Notably, treatment with TA-Zn-Gen 3 NPs reduced cfDNA to the non-CLP level (Figure 8A), demonstrating cfDNA scavenging by the NPs *in vivo*. To our surprise, treatment with the mixture of free components, TA/Gen/Zn, also reduced the cfDNA level in serum, possibly due to reduced release of cfDNA from damaged cells following the therapeutic effects of gentamicin and tannic acid. We used HEK-Blue hTLR9 cells to examine the inhibition of cfDNA-induced TLR9 activation by the NPs *in vivo*. The serum of TA-Zn-Gen 3 NP-treated mice showed the lowest TLR9 activation (Figure 8B), indicating reduction of cfDNA-induced TLR9 activation, consistent with the reduced cfDNA level in serum. A reduced fraction of M1 polarized macrophages was observed in both TA-Zn-Gen 3 NPs and TA/Gen/Zn treatment groups (Figure 8C), indicating inhibition of macrophage activation. We next assessed ROS levels in the treatment groups. In comparison with the untreated CLP group, TA-Zn-Gen 3 NPs and TA/Gen/Zn treatments reduced the fraction of cells with a high ROS level in the peritoneal cavity (Figures 8D, S19, and S20), indicating alleviation of inflammation at this site. The TA-Zn-Gen 3 NP treatment caused greater reduction in ROS than TA/Gen/Zn. The number of bacteria in the abdominal cavity was also evaluated. The fewest bacteria in the peritoneal cavity were observed in the TA-Zn-Gen 3 NP treatment group (Figures 8E and 8F), demonstrating the outstanding antibacterial effect of the NPs *in vivo*. Since cytokine release is a main consequence of TLR activation, the proinflammatory cytokines interleukin 6 (IL-6) and TNF-α, which are predominantly secreted by activated immune cells, were investigated. Large quantities of TNF-α and IL-6 were detected in the serum and peritoneal cavity of mice in the untreated CLP group (Figures 8G–8J). In contrast, both TA-Zn-Gen NPs and TA/Gen/Zn treatments showed decreased TNF-α and IL-6 levels in serum and peritoneum. The NPs caused a greater reduction of TNF-α and IL-6 than the mixture of components, possibly due to scavenging of cfDNA by the NPs.

Since multiple organ failure due to a ."cytokine storm is a primary clinical manifestation of severe sepsis, we examined the effects of the NPs on multiple organ injury by histopathological and biochemical analysis.[46] As shown in H&E staining images (Figure S21), typical characteristics of multiple organ injuries such as tissue destruction and leukocyte infiltration appeared in the heart, liver, lung, and kidney of mice in the untreated CLP group. Treatment with the TA/Gen/Zn mixture showed limited protective effect on organ damage, although this treatment alleviated inflammation. In contrast, and in agreement with the survival data, the TA-Zn-Gen 3 NPs appeared to reduce multiple organ injury as suggested by histological analysis. Consistently, blood biochemical analysis validated the protective effects of the TA-Zn-Gen 3 NPs in preventing major organ failure (Figure S22). No detectable side effect was observed in the organs of mice at 5 days after injection with the TA-Zn-Gen 3 NPs (Figure S23), indicating the low systemic toxicity of the TA-Zn-Gen 3 NPs. Collectively, the TA-Zn-Gen NPs displayed a more favorable therapeutic effect than the soluble mixture of components, demonstrating the importance of scavenging inflammatory cfDNA and prolonging retention time in inflamed tissues, and showing the potential for using multifunctional NPs that target multiple mediators of sepsis to improve sepsis treatment.

Conclusions
Here we developed multifunctional NPs consisting of tannic acid, Zn^{2+}, and gentamicin that attenuate both hyperinflammation and infection to improve sepsis treatment. The TA-Zn-Gen NPs bind inflammatory cfDNA, inhibit macrophage recruitment, scavenge detrimental ROS, modulate macrophage activation, and kill bacteria, thereby effectively eliminating multiple mediators of sepsis, resulting in

Matter
Article

CellPress

an attenuated inflammatory response. The TA-Zn-Gen NPs yielded 60% survival of CLP septic mice versus 40% for a soluble mixture of tannic acid, Zn^{2+}, and gentamicin, and 0% for untreated CLP mice. The NPs significantly ameliorated systemic inflammation as assessed by cytokine profiling, reduced TLR9 activation, and reduced organ failure. This robust protective effect of the TA-Zn-Gen NPs in a severe sepsis model suggests that using multifunctional NPs that scavenge or otherwise target multiple mediators of inflammation might provide a novel effective strategy for treating sepsis as well as many other inflammation-associated diseases.

EXPERIMENTAL PROCEDURES

Resource availability

Lead contact
Please contact Prof. Kam W. Leong via kam.leong@columbia.edu for further information.

Materials availability
The materials generated in this study are available from the corresponding author upon request.

Data and code availability
All data are available upon request to the lead contact.

Materials

Gentamicin sulfate, Zn(NO$_3$)$_2$·6H$_2$O, tannic acid, CuSO$_4$·5H$_2$O, H$_2$O$_2$ solution, *tert*-butyl hydroperoxide (TBHP), 2,2′-azobis(2-amidinopropane) dihydrochloride (AAPH), xanthine oxidase, xanthine, calf thymus DNA, hydroethidine, and transwell cell culture plate inserts were purchased from Sigma Aldrich. Cy7-NHS ester was purchased from Meilun, China. FBS, PBS, and DMEM were purchased from Gibco. HEK-Blue hTLR cell lines, Quanti-Blue, CpG Bw006, LPS, and Poly (I:C) were purchased from InvivoGen. Quant-iT PicoGreen dsDNA Assay Kit, 4′,6-diamidino-2-phenylindole (DAPI), and LysoTracker Red DND-99 were purchased from Invitrogen. Lipofectamine 3000, 2-(3,6-diacetyloxy-2,7-dichloro-9H-xanthen-9-yl) benzoic acid (H$_2$DCFDA), Nitric Oxide Assay Kits, and HCS DNA Damage Kits were purchased from Thermo Fisher Scientific. Total mRNA extraction kits, TIANScript II RT Kits, and SuperReal PreMix Plus (SYBR Green) were purchased from Tiangen, China. A DNA Blood Mini Kit was purchased from Qiagen, Germany. F4/80-PE-Cy7, CD11c-PE, and CD11b-FITC antibodies were purchased from eBioscience. TNF-α and glyceradehyde-3-phosphate dehydrogenase (GAPDH) primers were synthesized by Sangon Biotech, China. CCK-8 was purchased from Abcam.

Instruments

NP zeta potential and size were measured using a Malvern Zetasizer. UV-visible absorption spectra were obtained with a UV-1700 Spectrophotometer (Shimadzu, Japan). FTIR spectra were recorded using a Nicolet 520 FTIR spectrometer. Powder XRD (PXRD) spectra were obtained with a D8 ADVANCE X-ray diffractometer (40 kV, 40 mA). Zn content was determined by inductively coupled plasma atomic emission spectroscopy (ICP-MS, Thermo Scientific Xseries 2, Thermo Fisher Scientific). Elemental analysis results were measured with a VARIO EL-III Elemental Analyzer.

Preparation of TA-Zn-Gen NPs

Tannic acid solution (100 mg/mL), Zn (NO3)2·6H$_2$O solution (50 mg/mL), and different volumes (0.125, 0.25, 0.5, 1, and 2 mL for TA-Zn-Gen NPs #1–#5, respectively) of gentamicin solution (100 mg/mL) were continuously added to Milli-Q water to create a final

volume of 25 mL. The mixture was stirred at room temperature for 10 min, then the pH was adjusted to 5.2 using 10 M NaOH solution, and stirring was continued for another 20 min. The complex was then centrifuged at 8,000 rpm for 5 min, and the collected precipitate was washed with Milli-Q water three times. The precipitate was lyophilized with trehalose as a cryoprotectant for further use.

DNA binding affinity

Quant-iT PicoGreen (12.5 μL) and calf thymus DNA (5 mg/mL, 25 μL) were mixed with 1× TE buffer (10 mL) in the dark. NPs at different concentrations in 100 μL together with 100 μL of the above solution were added to a 96-well black plate and incubated at 37°C for 30 min. The fluorescence intensity of the Picogreen-DNA complex at 520 nm was measured with a multiwell plate reader (Bio-Tek, Winooski, VT) via excitation at 490 nm.

ROS scavenging

Hydroxyl radicals were generated by a Fenton reaction of $CuSO_4$ and H_2O_2. The amount of hydroxyl radical scavenged was calculated by measuring the characteristic absorbance of oxidized TMB (1 mM) at 650 nm in the presence of $CuSO_4$ (2 mM), H_2O_2 (5 mM), and NPs. Superoxide anions were generated by mixing xanthine oxidase (0.05 U/mL) and xanthine (0.6 mM) in PBS at 37°C for 40 min. NPs at different concentrations were added to the above solution and incubated for another 40 min, followed by adding hydroethidine at 0.5 mg/mL. The amount of superoxide anion scavenged was determined by measuring the fluorescent intensity of ethidium (oxidation product of hydroethidine by superoxide radical) at 610 nm with a multiwell plate reader via excitation at 470 nm.

Cytotoxicity assay

The cytotoxicity of NPs was evaluated with a CCK-8 assay. RAW 264.7 cells were plated into a 96-well plate at a density of 8,000 cells/well and were allowed to adhere overnight in growth medium at 37°C, 5% CO_2. The cells were then treated with NPs at different concentrations and cultured for another 24 h. The medium was replaced with medium containing 10% CCK-8 (100 μL), and cell viability was determined with a multiwell plate reader by measuring the OD at 490 nm.

Colocalization of NPs and CpG in cells

RAW 264.7 cells were seeded on coverslips in a 12-well plate at 5×10^4 cells/well and were allowed to adhere overnight in growth medium at 37°C, 5% CO_2. Next, 1 μg/mL of Cy5.5-labeled CpG 1826 was added for 30 min. Then the cells were washed with PBS three times and were cultured with FITC-labeled NPs (100 μg/mL) for another 12 h. The cells were then stained with DAPI and LysoTracker Red DNA-99, washed repeatedly with PBS, mounted on slides with mounting medium, and imaged with a Nikon structured illumination microscope.

Transfection of plasmid green fluorescent protein (pGFP) by TA-Zn-Gen 3 NPs

HEK 293 cells were seeded in a 24-well plate at 2×10^5 cells/well and were allowed to adhere overnight in growth medium at 37°C, 5% CO_2. Next, the cells were treated with a pre-mixed solution of plasmid (1 μg/well) and TA-Zn-Gen 3 at different NPs concentrations and were cultured for another 24 h. For the positive control group, Lipofectamine 3000 was used. The effect of the NPs on transfection was determined by green fluorescence intensity using a fluorescence microscope.

Matter
Article

Inhibition of agonist-induced TLR3, TLR4, and TLR9 activation by NPs

HEK-Blue hTLR cells were cultured and maintained in DMEM with 10% FBS and 1% penicillin-streptomycin. To evaluate NPs inhibition of TLR activation, HEK-Blue hTLR cells were seeded in a 96-well plate for 30 min then treated with 2 μL of agonist (CpG Bw006 or Poly (I:C), 1 mg/mL; LPS, 100 ng/mL). After 20 min of incubation, 2 μL of NPs at different concentrations were introduced in a final volume of 200 μL. After 24 h, the supernatants were collected and mixed with Quanti-Blue. TLR activation associated with SEAP activity was determined with a multiwell plate reader by measuring the OD at 620 nm. The cell densities (in a 96-well plate) and agonists used were 8×10^4 cells/well and CpG Bw006 for HEK-Blue hTLR9 cells, 5×10^4 cells/well and Poly (I:C) for HEK-Blue hTLR3 cells, and 2.5×10^4 cells/well and LPS for HEK-Blue hTLR4 cells.

In vitro anti-inflammatory assay

RAW 264.7 macrophages were seeded in a 96-well plate at 2×10^4 cells/well and after 30 min of incubation were treated with 2 μL of CpG Bw006 (1 mg/mL). After another 20 min, 2 μL of NPs at different concentrations were added in a final volume of 200 μL. After incubation for another 24 h, the supernatants were collected and assessed with a TNF-α ELISA kit.

Quantitative real-time PCR assay in vitro

RAW 264.7 cells were seeded in a 6-well plate at 5×10^5 cells/well for 30 min, then CpG Bw006 or LPS was added (final concentration: CpG Bw006, 1 μg/mL; LPS, 10 ng/mL). The NPs were added at a final concentration of 100 μg/mL after 20 min of incubation. After 24 h, total mRNA was exacted and reverse transcribed to cDNA with a total mRNA extraction kit and a TIANScript II RT Kit, respectively. qPCR was then performed using SuperReal PreMix Plus (SYBR Green) on a qPCR machine (Roche Diagnostics Ltd, Lewes, UK). Amplified transcripts were quantified using the comparative cycle threshold (Ct) method.

Intracellular ROS assay

For imaging ROS levels, RAW 264.7 cells were seeded in 12-well plates (1×10^5/well) and were allowed to adhere overnight in growth medium (37°C, 5% CO$_2$). The cells were then treated with 1 mM TBHP for 4 h. Following three washes with PBS, the cells were treated with NPs for another 24 h. After staining with H$_2$DCFDA and DAPI, the cells were washed repeatedly with PBS and were imaged using a fluorescence microscope.

Protection from ROS-induced DNA damage

Supercoiled pGFP plasmid DNA (0.05 μg/mL, 2 μL), NPs (100 μg/mL, 2 μL), AAPH (10 mM, 4 μL), and PBS (2 μL) were mixed and incubated at 37°C for 1 h. After mixing with 1× loading buffer (2 μL), the samples were analyzed by electrophoresis in 1% agarose gels stained with ethidium bromide for 1 h (buffer: 45 mM Tris-borate, 1 mM EDTA, pH 8). After electrophoresis, the gels were illuminated with a UV transilluminator and photographed, and band intensities were analyzed using ImageJ software.

DNA damage imaging

RAW 264.7 cells were seeded on coverslips in a 96-well plate at 2×10^4 cells/well and were allowed to adhere overnight in growth medium at 37°C, 5% CO$_2$. The cells were then treated with 50 μM H$_2$O$_2$ and NPs (50 μg/mL) for 24 h. For the control group, no H$_2$O$_2$ and NPs were added; for the positive control group, only H$_2$O$_2$

was added. Following staining with DAPI and HSC DNA Damage Kit, the cells were washed with PBS and imaged with a fluorescence microscope.

Protection from ROS-induced cell death

RAW 264.7 cells were plated in a 96-well plate at 8,000 cells/well and were allowed to adhere overnight in growth medium at 37°C, 5% CO$_2$. The cells were then treated with H$_2$O$_2$ (100 μM) and NPs at different concentrations for 24 h. For the control group, no H$_2$O$_2$ and NPs were added; for the positive control group, only H$_2$O$_2$ was added. Next, the medium was replaced with medium containing 10% CCK-8 (100 μL). The viability of cells was determined with a multiwell plate reader by measuring the OD at 490 nm.

In vitro anti-macrophage migration activity of TA-Zn-Gen NPs

A transwell assay was conducted to investigate the anti-macrophage migration activity of the TA-Zn-Gen NPs. RAW 264.7 cells were seeded in a 24-well plate at 2.5 × 10^5 cells/well and were allowed to adhere overnight in growth medium at 37°C, 5% CO$_2$. Then the cells were treated with CpG Bw006 for 4 h. Following repeated washes with PBS and adding growth medium without FBS, 8-μm pore polycarbonate transwell chambers containing resuspended RAW 264.7 cells (2.5 × 10^5 cells, 0.2 mL) were inserted into the wells. Next, the cells were treated with NPs for 24 h. For the negative control group, no CpG Bw006 or NPs were added; for the positive control group, only CpG Bw006 was added; for the experimental groups, both CpG Bw006 and NPs were added. After cells were allowed to migrate for 24 h, cells on the upper side of each insert were gently removed with a cotton swab. Subsequently, the migrated cells on the lower side of each insert were fixed and stained with 0.1% crystal violet. Then, five images of migrated stained cells per high-power field fixed on the lower side of chamber were acquired for microscopic analysis.

Inhibition of LPS-induced nitric oxide generation

RAW 264.7 cells were seeded in a 96-well plate at 4 × 10^4 cells/well and were allowed to adhere overnight in growth medium at 37°C, 5% CO$_2$. The cells were treated with LPS (10 ng/mL) and NPs (50 μg/mL or 100 μg/mL) for 24 h. For the negative control group, no LPS and NPs were added; for the positive control group, only LPS was added. Then the supernatants were collected and mixed with an NO assay kit, and nitric oxide generation was determined with a multiwell plate reader.

Antibacterial effect of NPs

E. coli diluted in Luria-Bertani liquid medium were seeded in a 96-well plate at a density of 10^6/mL and were treated with NPs at different concentrations. After 6 h and 12 h of incubation with NPs at 37°C, the proliferation of bacteria was determined with a multiwell plate reader by measuring the OD at 600 nm.

Establishment of CLP-induced sepsis model

C57 mice (male, 6 or 8 weeks old) were purchased from Liaoning Changsheng Biotechnology. All animal experiments were conducted according to the guidelines for laboratory animals established by the Animal Care and Use Committee of Jilin University. The CLP-induced sepsis model was established as described previously.[47] Briefly, mice were anesthetized using an isoflurane anesthesia system, followed with abdominal hair shaving and disinfection. Next, the cecum was gently exteriorized after a 1-cm incision at the midline. After ligation with 4-0 silk at the designated position for severe grade sepsis, the cecum was punctured with a 21-gauge needle and the cecal content was extruded through the perforation. The

cecum was then put back into the peritoneal cavity followed by stitching of the incision.

Treatment of CLP-induced sepsis mice

C57 mice were divided into control, sham, CLP, TA/Gen/Zn, and TA-Zn-Gen 3 NP groups (10 mice per group). Mice in the CLP group underwent the CLP procedure described above without further treatment. Mice in the sham group underwent only the abdominal laparotomy procedure without subsequent CLP. In the TA/Gen/Zn and TA-Zn-Gen 3 NPs groups, TA/Gen/Zn or TA-Zn-Gen 3 NPs were administered at 10 mg/kg at 1 h and 12 h after CLP. TA/Gen/Zn is a soluble mixture of tannic acid, gentamicin, and Zn^{2+}, and the dosage of each component is the same as in the TA-Zn-Gen 3 NPs. The clinical scores, survival rate, and body weight were monitored for five consecutive days. The criteria of clinical score according to a previously established method were listed as follows: 0, no symptoms; 1, piloerection and huddling; 2, piloerection, diarrhea, and huddling; 3, lack of interest in surroundings and severe diarrhea; 4, decreased movement and listless appearance; 5, loss of self-righting reflex. Mice were humanely killed when they exhibited a score of 5.

Ex vivo fluorescence imaging

The mice were injected intraperitoneally with Cy7-labeled TA-Zn-Gen 3 NPs at 10 mg/kg at 1 h post CLP. The major organs and cecum were collected at 2 h, 12 h, and 24 h post CLP and were imaged with an *in vivo* imaging system.

Fraction of M1 polarized macrophages in peritoneal cavity

The fraction of M1 polarized macrophages in the peritoneal cavity was evaluated by flow cytometry. Briefly, a peritoneal lavage was performed with 5 mL of PBS containing 10% FBS, and the cells were collected and stained with anti-CD11b-FITC, anti-CD11c-PE, and anti-F4/80-PE-Cy7 antibodies at 4°C for 1 h. As previously reported in the literature, the CD11b and F4/80 dual-positive cells represent the microphages, and the CD11b, F4/80, and CD11c triple-positive cells represent the M1-polarized macrophages. The X axis (CD11b + F4/80 + CD11c+) in Figure 8C indicated the CD11b, F4/80, and CD11c triple-positive cells. After repeated washes with PBS, the cells were analyzed with a BD FACS Celesta multicolor cell analyzer.

Fraction of cells with high ROS level in peritoneal cavity

The fraction of cells with a high ROS level in the peritoneal cavity was evaluated by flow cytometry. Briefly, a peritoneal lavage was performed with 5 mL of PBS containing 10% FBS, and the cells in lavage were collected and stained with an ROS kit at 4°C for 2 h. After repeated washes with PBS, the cells were analyzed with a BD FACS Celesta multicolor cell analyzer.

Extraction and quantification of cfDNA

cfDNA from serum and peritoneal lavage fluid was extracted with a QIAamp DNA Blood Mini Kit and were quantified with a Quant-iT PicoGreen dsDNA Assay Kit.

Number of bacteria in peritoneal cavity

A peritoneal lavage of mice in different groups was diluted and plated on Luria-Bertani solid medium. After 24 h of incubation at 37°C, colony forming units (CFU) were counted.

Activation of TLR9/MyD88/NF-κB pathway by serum from treated mice

HEK-Blue hTLR9 cells were seeded in a 96-well plate at 8×10^4 cells/well without FBS for 30 min and were then treated with 10 μL of serum from mice in different

🧀 **CellPress**

Matter
Article

groups. After 24 h of incubation, the supernatants were collected and mixed with Quanti-Blue. The activation of TLR9/MyD88/NF-κB pathway associated with SEAP activity was determined with a multiwell plate reader by measuring the OD at 620 nm.

SUPPLEMENTAL INFORMATION

Supplemental information can be found online at https://doi.org/10.1016/j.matt.2021.09.001.

AUTHOR CONTRIBUTIONS

F.L., H.T., and K.W.L. conceived and designed the study. F.L., Y.W., and S.S. synthesized and characterized the materials. F.L., S.S., Y.X., Y.Z., J.Z., C.H.Q., J.D., and C.Y. contributed to cell and animal experiments. F.L., S.S., D.D., H.T., and K.W.L. analyzed the data. F.L., H.T., and K.W.L. co-wrote the paper. All authors discussed the results and commented on the manuscript.

DECLARATION OF INTERESTS

The authors declare no competing interests.

REFERENCES

1. Hotchkiss, R.S., Moldawer, L.L., Opal, S.M., Reinhart, K., Turnbull, I.R., and Vincent, J.L. (2016). Sepsis and septic shock. Nat. Rev. Dis. Primers 2, 16045.

2. Angus, D.C., and van der Poll, T. (2013). Severe sepsis and septic shock. N. Engl. J. Med. 369, 840–851.

3. Arnold, C. (2018). News Feature: the quest to solve sepsis. Proc. Natl. Acad. Sci. U S A 115, 3988–3991.

4. Stearns-Kurosawa, D.J., Osuchowski, M.F., Valentine, C., Kurosawa, S., and Remick, D.G. (2011). The pathogenesis of sepsis. Annu. Rev. Pathol. Mech. Dis. 6, 19–48.

5. Goldenberg, N.M., Steinberg, B.E., Slutsky, A.S., and Lee, W.L. (2011). Broken barriers: a new take on sepsis pathogenesis. Sci. Transl. Med. 3, 88ps25.

6. Beishuizen, A., Vermes, I., and Haanen, C. (1998). Endogenous mediators in sepsis and septic shock. Adv. Clin. Chem. 33, 55–131.

7. Jaber, B.L., and Pereira, B.J.G. (1996). Inflammatory mediators in sepsis: rationale for extracorporeal therapies? Am. J. Kidney Dis. 28, S35–S49.

8. Mosevoll, K.A., Skrede, S., Markussen, D.L., Fanebust, H.R., Flaatten, H.K., Aßmus, J., Reikvam, H., and Bruserud, Ø. (2018). Inflammatory mediator profiles differ in sepsis patients with and without bacteremia. Front. Immunol. 9, 691.

9. Harrison, C. (2010). Sepsis: calming the cytokine storm. Nat. Rev. Drug Discov. 9, 360–361.

10. Wang, H., and Ma, S. (2008). The cytokine storm and factors determining the sequence and severity of organ dysfunction in multiple organ dysfunction syndrome. Am. J. Emerg. Med. 26, 711–715.

11. Marsman, G., Zeerleder, S., and Luken, B.M. (2016). Extracellular histones, cell-free DNA, or nucleosomes: differences in immunostimulation. Cell Death Dis. 7, e2518.

12. Timmermans, K., Kox, M., Scheffer, G.J., and Pickkers, P. (2016). Plasma nuclear and mitochondrial DNA levels, and markers of inflammation, shock, and organ damage in patients with septic shock. Shock 45, 607–612.

13. Rhodes, A., and Cecconi, M. (2012). Cell-free DNA and outcome in sepsis. Crit. Care 16, 170.

14. Lee, J., Sohn, J.W., Zhang, Y., Leong, K.W., Pisetsky, D., and Sullenger, B.A. (2011). Nucleic acid-binding polymers as anti-inflammatory agents. Proc. Natl. Acad. Sci. U S A 108, 14055–14060.

15. Holl, E.K., Shumansky, K.L., Borst, L.B., Burnette, A.D., Sample, C.J., Ramsburg, E.A., and Sullenger, B.A. (2016). Scavenging nucleic acid debris to combat autoimmunity and infectious disease. Proc. Natl. Acad. Sci. U S A 113, 9728–9733.

16. Dawulieti, J., Sun, M., Zhao, Y., Shao, D., Yan, H., Lao, Y.-H., Hu, H., Cui, L., Lv, X., Liu, F., et al. (2020). Treatment of severe sepsis with nanoparticulate cell-free DNA scavengers. Sci. Adv. 6, eaay7148.

17. Liang, H., Peng, B., Dong, C., L, L., Mao, J., Wei, S., Wang, X., Xu, H., Shen, J., Mao, H.-Q., et al. (2018). Cationic nanoparticle as an inhibitor of cell-free DNA-induced inflammation. Nat. Commun. 9, 4291.

18. Jones, C.F., Campbell, R.A., Brooks, A.E., Assemi, S., Tadjiki, S., Thiagarajan, G.,

Matter
Article

CellPress

Mulcock, C., Weyrich, A.S., Brooks, B.D., Ghandehari, H., et al. (2012). Cationic PAMAM dendrimers aggressively initiate blood clot formation. ACS Nano 6, 9900–9910.

19. Ohto, U., Fukase, K., Miyake, K., and Shimizu, T. (2012). Structural basis of species-specific endotoxin sensing by innate immune receptor TLR4/MD-2. Proc. Natl. Acad. Sci. U S A 109, 7421.

20. Beutler, B., and Rietschel, E.T. (2003). Innate immune sensing and its roots: the story of endotoxin. Nat. Rev. Immunol. 3, 169–176.

21. Maysinger, D., Hébert, M.L., Ji, J., Jabbour, K., Dernedde, J., Silbereis, K., Haag, R., and Kriz, J. (2019). Dendritic polyglycerols are modulators of microglia-astrocyte crosstalk. Future Neurol. 14, FNL31.

22. Wittebole, X., Castanares-Zapatero, D., and Laterre, P.F. (2010). Toll-like receptor 4 modulation as a strategy to treat sepsis. Mediators Inflamm. 2010, 568396.

23. Lima, C.X., Souza, D.G., Amaral, F.A., Fagundes, C.T., Rodrigues, I.P.S., Alves-Filho, J.C., Kosco-Vilbois, M., Ferlin, W., Shang, L., Elson, G., and Teixeira, M.M. (2015). Therapeutic effects of treatment with anti-TLR2 and anti-TLR4 monoclonal antibodies in polymicrobial sepsis. PLoS One 10, e0132336.

24. Solov'eva, T., Davydova, V., Krasikova, I., and Yermak, I. (2013). Marine compounds with therapeutic potential in gram-negative sepsis. Mar. Drugs 11, 2216–2229.

25. Cao, F., Zhang, L., You, Y., Zheng, L., Ren, J., and Qu, X. (2020). An enzyme-mimicking single-atom catalyst as an efficient multiple reactive oxygen and nitrogen species scavenger for sepsis management. Angew. Chem. Int. Ed. 59, 5108–5115.

26. Rittirsch, D., Flierl, M.A., and Ward, P.A. (2008). Harmful molecular mechanisms in sepsis. Nat. Rev. Immunol. 8, 776–787.

27. Hassan, F.I., Didari, T., Khan, F., Niaz, K., Mojtahedzadeh, M., and Abdollahi, M. (2020). A review on the protective effects of metformin in sepsis-induced organ failure. Cell J. 21, 363–370.

28. Dinarello, C.A. (2001). Anti-cytokine therapies in response to systemic infection. J. Invest. Dermatol. Symp. Proc. 6, 244–250.

29. Roger, T., Froidevaux, C., Le Roy, D., Reymond, M.K., Chanson, A.-L., Mauri, D., Burns, K., Riederer, B.M., Akira, S., and Calandra, T. (2009). Protection from lethal gram-negative bacterial sepsis by targeting toll-like receptor 4. Proc. Natl. Acad. Sci. U S A 106, 2348.

30. Fisher, C.J., Agosti, J.M., Opal, S.M., Lowry, S.F., Balk, R.A., Sadoff, J.C., Abraham, E., Schein, R.M., and Benjamin, E. (1996). Treatment of septic shock with the tumor necrosis factor receptor:Fc fusion protein. N. Engl. J. Med. 334, 1697–1702.

31. Opal, S.M., Fisher, C.J.J.r., Dhainaut, J.F., Brase, R., Lowry, S.F., Sadoff, J.C., Slotman, G.J., Levy, H., Balk, R.A., Shelly, M.P., et al. (1997). Confirmatory interleukin-1 receptor antagonist trial in severe sepsis: a phase III, randomized, doubleblind, placebo-controlled, multicenter trial. Crit. Care Med. 25, 1115–1124.

32. Shi, C., Wang, X., Wang, L., Meng, Q., Guo, D., Chen, L., Dai, M., Wang, G., Cooney, R., and Luo, J. (2020). A nanotrap improves survival in severe sepsis by attenuating hyperinflammation. Nat. Commun. 11, 3384.

33. Jin, Q., Deng, Y., Chen, X., and Ji, J. (2019). Rational design of cancer nanomedicine for simultaneous stealth surface and enhanced cellular uptake. ACS Nano 13, 954–977.

34. Abouelmagd, S.A., Abd Ellah, N.H., Amen, O., Abdelmoez, A., and Mohamed, N.G. (2019). Self-assembled tannic acid complexes for pH-responsive delivery of antibiotics: role of drug-carrier interactions. Int. J. Pharm. 562, 76–85.

35. Takeshita, F., Takeshita, F., Gursel, I., Ishii, K.J., Suzuki, K., Gursel, M., and Klinman, D.M. (2004). Signal transduction pathways mediated by the interaction of CpG DNA with toll-like receptor 9. Semin. Immunol. 16, 17–22.

36. Tsujimoto, H., Ono, S., Efron, P.A., Scumpia, P.O., Moldawer, L.L., and Mochizuki, H. (2008). Role of toll-like receptors in the development of sepsis. Shock 29, 315–321.

37. Zha, Z., Yue, X., Ren, Q., and Dai, Z. (2013). Uniform polypyrrole nanoparticles with high photothermal conversion efficiency for photothermal ablation of cancer cells. Adv. Mater. 25, 777–782.

38. Atalan, N., Acar, L., Yapic, N., Kudsioglu, T., Ergen, A., Yilmaz, S.G., and Isbir, T. (2018). The relationship between sepsis-induced immunosuppression and serum toll-like receptor 9 level. In Vivo 32, 1653–1658.

39. Guo, J., Li, D., Tao, H., Li, G., Liu, R., Dou, Y., Jin, T., Li, L., Huang, J., Hu, H., and Zhang, J. (2019). Cyclodextrin-derived intrinsically bioactive nanoparticles for treatment of acute and chronic inflammatory diseases. Adv. Mater. 31, 1904607.

40. Mantzarlis, K., Tsolaki, V., and Zakynthinos, E. (2017). Role of oxidative stress and mitochondrial dysfunction in sepsis and potential therapies. Oxid. Med. Cell Longev. 2017, 5985209.

41. Yao, J., Cheng, Y., Zhou, M., Zhao, S., Lin, S., Wang, X., Wu, J., Li, S., and Wei, H. (2018). ROS scavenging Mn₃O₄ nanozymes for in vivo anti-inflammation. Chem. Sci. 9, 2927–2933.

42. Li, Y., Li, Z., Hou, H., Zhuang, Y., and Sun, L. (2018). Metal chelating, inhibitory DNA damage, and anti-inflammatory activities of phenolics from rambutan (*Nephelium lappaceum*) peel and the quantifications of geraniin and corilagin. Molecules 23, 2263.

43. Natale, F., Rapp, A., Yu, W., Maiser, A., Harz, H., Scholl, A., Grulich, S., Anton, T., Horl, D., Chen, W., et al. (2017). Identification of the elementary structural units of the DNA damage response. Nat. Commun. 8, 15760.

44. Jones, E., Adcock, I.M., Ahmed, B.Y., and Punchard, N.A. (2007). Modulation of LPS stimulated NF-kappaB mediated nitric oxide production by PKCε and JAK2 in RAW macrophages. J. Inflamm. 4, 23.

45. Hu, D., Yang, X., Xiang, Y., Li, H., Yan, H., Zhou, J., Caudle, Y., Zhang, X., and Yin, D. (2015). Inhibition of Toll-like receptor 9 attenuates sepsis-induced mortality through suppressing excessive inflammatory response. Cell Immunol. 295, 92–98.

46. Chousterman, B.G., Swirski, F.K., and Weber, G.F. (2017). Cytokine storm and sepsis disease pathogenesis. Semin. Immunopathol. 39, 517–528.

47. Rittirsch, D., Huber-Lang, M.S., Flierl, M.A., and Ward, P.A. (2009). Immunodesign of experimental sepsis by cecal ligation and puncture. Nat. Protoc. 4, 31–36.